J Fluoresc (2007) 17:687–699
DOI 10.1007/s10895-007-0217-x

ORIGINAL PAPER

Segmented Frequency-domain Fluorescence Lifetime Measurements: Minimizing the Effects of Photobleaching Within a Multi-component System

Hadi M. Marwani · Mark Lowry · Patrick Keating · Isiah M. Warner · Robert L. Cook

Received: 11 December 2006 / Accepted: 4 June 2007 / Published online: 23 August 2007

Abstract This study introduces a newly developed frequency segmentation and recombination method for frequency-domain fluorescence lifetime measurements to address the effects of changing fractional contributions over time and minimize the effects of photobleaching within multi-component systems. Frequency segmentation and recombination experiments were evaluated using a two component system consisting of fluorescein and rhodamine B. Comparison of experimental data collected in traditional and segmented fashion with simulated data, generated using different changing fractional contributions, demonstrated the validity of the technique. Frequency segmentation and recombination was also applied to a more complex system consisting of pyrene with Suwannee River fulvic acid reference and was shown to improve recovered lifetimes and fractional intensity contributions. It was observed that photobleaching in both systems led to errors in recovered lifetimes which can complicate the interpretation of lifetime results. Results showed clear evidence that the frequency segmentation and recombination method reduced errors resulting from a changing fractional contribution in a multi-component system, and allowed photobleaching issues to be addressed by commercially available instrumentation.

Keywords Time-resolved fluorescence · Frequency-domain lifetime measurements · Frequency segmentation · Photobleaching · Multi-component system · Data analysis

Introduction

Time-resolved measurements are commonly used in fluorescence spectroscopy, especially for biological applications [1]. Fluorescence lifetime measurements are also used in analytical applications as a tool for selectivity enhancement and determinations in multi-component systems [2]. These measurements provide important information such as the rates of excited-state reactions, energy transfer between donor and acceptor molecules, and fluorescence quenching in bimolecular processes [3]. In addition, fluorescence lifetime measurements are a powerful tool for distinguishing static from dynamic quenching.

One problem often encountered in fluorescence spectroscopy is the effect of photobleaching. Photobleaching is a chemical transformation of an excited fluorophore into a non-fluorescent component [4, 5]. Many studies have reported that photobleaching or photodegradation can affect the observed probe's fluorescence lifetime [6–12]. For example, Rueck et al. [11] used time-correlated single photon counting to investigate 5-aminolevulinic acid metabolites in solutions and cell cultures and observed a significant decrease in recovered lifetimes during illumination. Nakamura et al. [6] examined chlorophyll A in a droplet of *n*-octanol using time-resolved fluorescence microscopy and noted an increase in the shorter lived fraction with increasing exposure to radiation, but observed no effect on the recovered lifetimes of two decay components. Connelly et al. [12] used time-resolved fluorescence imaging to investigate photosensitiser distributions in

Electronic supplementary material The online version of this article doi:10.1007/s10895-007-0217-x contains supplementary material, which is available to authorized users.

H. M. Marwani · M. Lowry · P. Keating · I. M. Warner · R. L. Cook (✉)
Department of Chemistry, Louisiana State University, Baton Rouge, LA 70803, USA
e-mail: rlcook@lsu.edu

R. L. Cook
Department of Chemistry, Southern University at Baton Rouge, Baton Rouge, LA 70813, USA

mammalian cells. Their results suggested that photobleaching of *meta*-tetra(hydroxyphenyl) chlorine (*m*-THPC) led to artifacts in the lifetime analysis which shortened the recovered lifetime of *m*-THPC. Thus, photobleaching within multi-component systems can complicate the interpretation of fluorescence lifetimes and fractional intensity contributions by directly affecting the recovered values.

Photobleaching can also affect fluorescence lifetime measurements of complex fluorescent molecules having more than one fluorophore, such as collagen and elastin [13, 14]. Marcu et al. [9] investigated the photobleaching characteristics of the major fluorescent components (elastin, collagen, and cholesterol) of the arterial wall during prolonged exposure to nitrogen laser pulses at various fluence levels. It was observed that photobleaching of cholesterol was significant while that of elastin was less significant. The authors also reported that the fluorescence decay parameters of collagen and cholesterol varied with time when the fluence level of the excitation source was 21.75 μW/mm^2. A progressive decrease in the fluorescence lifetime with exposure time was observed. The photobleaching effect in time resolved measurements has generally been minimized by controlling the fluence level of the excitation source [9, 12]. In addition, photobleaching has a large effect in fluorescence lifetime imaging microscopy investigations [15–18]. The problem has also been addressed by reducing the fluence level but the issue has not been fully resolved. Decreasing the fluence level of the excitation source reduces signal intensity and may not be practical in all cases.

Problems with photobleaching have also been encountered in environmental applications of fluorescence, as exemplified by the application of fluorescence to studies of the association mechanism between hydrophobic organic compounds (HOC) and dissolved humic materials (DHM) [19–21]. Despite time-resolved fluorescence lifetime measurements [22, 23], the seemingly simple question of whether the quenching mechanism of HOC with DHM is static, dynamic, or both, is still open as the role of photobleaching has not been fully resolved.

In this study, the effect of photobleaching in multi-component systems was examined by frequency-domain fluorescence lifetime measurements *using a newly developed* frequency segmentation and recombination method. This technique is applicable on currently available frequency-domain lifetime instruments, and can be viewed as an alternative to specialized multi-harmonic frequency instrumentation (no such instrument is currently commercially available, e.g. SLM-Amico 48000 MHF) in terms of overcoming photobleaching. This method was investigated by simulation of a two component dye system consisting of fluorescein (Fl) and rhodamine B (RhB) and comparison of experimental data collected in traditional and segmented fashion. Additionally, the newly developed method was applied to a more complex system containing pyrene and Suwannee River fulvic acid reference (SRFAR) in order to carefully quantify recovered lifetimes and fractional intensity contributions.

Theory

Lifetime measurements In frequency-domain fluorescence lifetime measurements, sinusoidally modulated radiation excites the sample at high frequency. As a result, the emission response of the sample is also sinusoidally modulated at the same angular modulation frequency, ω, but out of phase with the excitation light. For a multi-component system, containing multiple discrete components, the fluorescence lifetime is the sum of exponential decays. The phase (ϕ) and demodulation (m) are functions of the ω, the lifetimes of each component (τ_i), and the fractional intensity contributions (α_i) of terms i:

$$\phi = \tan^{-1}\left(N_{\omega;}/D_\omega\right) \tag{1}$$

$$m = \left(N_\omega^2 + D_\omega^2\right)^{1/2} \tag{2}$$

where

$$N_\omega = \sum_i^n \frac{\alpha_i \omega \tau_i}{1+\omega^2\tau_i^2} \tag{3}$$

$$D_\omega = \sum_i^n \frac{\alpha_i}{1+\omega^2\tau_i^2} \tag{4}$$

The sum in Eqs. 3 and 4 corresponds to a system consisting of a finite number of components (n). By substituting Eqs. 3 and 4 into Eqs. 1 and 2, one can obtain both ϕ and m as a function of ω for a single exponential decay, containing one discrete component, as follows:

$$\phi = \tan^{-1}\left(\omega\tau\right) \tag{5}$$

and

$$m = \left(1+\omega^2\tau_m^2\right)^{-1/2} \tag{6}$$

where τ is the lifetime of the fluorophore. From Eqs. 5 and 6, it can be noted that short lifetimes require higher frequencies to interrogate the region of greatest change in ϕ and m. The opposite is true for long lifetimes [1, 24].

Fluorescence lifetime data analysis Non-linear least squares (NLLS) analysis is one of the most reliable and widely used methods for curve fitting. It allows one to obtain the parameters that minimize the quantity causing the mismatch between the measured and calculated values of the phase

and modulation. This can be achieved by minimizing the χ^2 parameter, which is obtained as follows:

$$\chi^2 = \frac{1}{v}\sum_{\omega}\left[\left(\frac{\phi-\phi_{c_\omega}}{\sigma_{\phi,\omega}}\right)^2+\left(\frac{m-m_{c_\omega}}{\sigma_{m,\omega}}\right)^2\right] \quad (7)$$

where v is the number of degrees of freedom, ϕ_{c_ω} and m_{c_ω} denote the calculated phase shift and demodulation value, and $\sigma_{\phi,\omega}$ and $\sigma_{m,\omega}$ are the errors associated with phase and modulation, respectively. Constant error values are often assumed for consistency and ease of day-to-day data interpretation. A valid model should usually provide a χ^2 value between 1 and 2. However, it is not possible to obtain χ^2 values within this range for some models of many complex systems. In such cases, χ^2 values alone cannot be used to statistically reject a model and residuals must be taken into consideration in model discrimination [1, 25].

Experimental section

Materials Fl (99%), RhB (~95%), and pyrene (≥99%) were obtained from Sigma-Aldrich (Milwaukee, WI) and used as received. SRFAR was purchased from the International Humic Substances Society (IHSS), Department of Soil, Water, and Climate, University of Minnesota (St. Paul, MN).

Sample preparation Standard reference solutions of 0.02 μM Fl, 1 μM RhB, and their mixture at the same concentrations were prepared in 0.1 M NaOH. Fluorescence measurements of Fl, RhB, and their mixture were collected on air-saturated samples to increase photobleaching as compared to deoxygenated systems.

Standard reference solutions of 0.1 ppm pyrene and 12 ppm SRFAR were prepared in 18.2 MΩ·cm distilled deionized water. The pyrene-SRFAR mixture, containing 0.04 ppm pyrene and 12 ppm SRFAR, was also prepared as above and stored in the dark at 4°C. The mixture was allowed to equilibrate in the dark for at least 7 days. Solutions were allowed to equilibrate overnight in a quartz fluorometer cell with septum cap and rinsed with fresh solutions prior to fluorescence measurements to reduce losses of pyrene to the cell wall. Individual reference solutions and mixture of pyrene and SRFAR were purged with argon gas for exactly 15 min followed by 5 min of equilibration time in the sample compartment with a flow of the argon gas prior to fluorescence measurements. The sample compartment was purged with argon gas during all measurements for such deoxygenated systems.

Methods All fluorescence measurements were acquired using a Spex Fluorolog-3 spectrofluorometer (model FL3-22TAU3; Jobin Yvon, Edison, NJ, USA) equipped with a 450-W xenon lamp and R928P photomultiplier tube (PMT) detector. Fluorescence measurements were made at room temperature in a 10 mm quartz fluorometer cell with septum cap. The excitation wavelength was 490 nm for Fl, RhB, and their mixture. Pyrene, SRFAR, and their mixture were excited at 333 nm. Time-based fluorescence steady-state experiments used to investigate the photostability of Fl and RhB were acquired with excitation bandpass set at 8.0 nm and emission bandpass at 2.0 nm. The emission was monitored at 512 and 576 nm for Fl and for RhB, respectively. Frequency-domain fluorescence signals were passed through 370 and 500 nm long-pass filters for pyrene and dye solutions, respectively. Frequency-domain fluorescence lifetime experimental details including frequency range, number of frequencies, averages, and integration times for both long and combined run segments are provided in Table 1. For the long run, an integration time of 30 and 15 s were used for Fl/RhB and Pyrene/SRFAR systems, respectively. The combined runs are a combination of four individual segments, with a fresh solution used for each segment. Frequency-domain measurements were collected for all solutions versus ludox—a scatter reference solution—which shows a lifetime of zero. Frequency-domain phase and modulation decay profiles were analyzed using the Globals software package developed at the Laboratory for Fluorescence Dynamics at the University of Illinois at Urbana–Champaign [26, 27]. Several initial guesses of parameters were implemented using NLLS analysis to examine the stability of the χ^2 minimization. Phase and modulation data sets were well fit by appropriate models as indicated by visual inspection of residual plots as well as by χ^2 statistics. Constant errors of 0.5° and 0.005 were used in analyses for consistency and ease of day-to-day data interpretation.

Table 1 Frequency-domain fluorescence lifetime experimental details of the LR and four CR segments

Set	Range (MHz)	Number	Time (s)	Averages	Time exposed (min)
LR	0.5–275.4	39	15.0 or 30.0	5	29.25 or 58.50
CR (segment 1)	4.3–233.3	13	15.0	5	9.75
CR (segment 2)	0.5–19.3	12	15.0	5	9.00
CR (segment 3)	0.6–3.1	6	30.0	5	9.00
CR (segment 4)	26.9–275.4	8	7.5	5	3.00

The frequency range is in the logarithmic scale. Averages are calculated using the interleave function such that an average is generated each time the automated sample turret rotates.

Results and discussion

Photobleaching and lifetime measurements In frequency-domain fluorescence lifetime measurements, the phase difference and demodulation of the sample are typically recorded at several modulation frequencies as the frequency is sequentially varied in a long run. The modulation frequency is generally increased from the lowest to highest frequency. Thus, measurements made at the highest frequency are performed on a solution which has been exposed to the greatest amount of radiation. Consequently, photobleaching of one component in a multi-component system can change fractional intensity contributions of all components over the course of the measurement, leading to errors in both recovered fractions and lifetimes. In order to reduce photobleaching one must minimize the amount of light to which the sample is exposed. This can be addressed to a certain level via hardware improvements.

Conventional frequency-domain fluorescence lifetime measurements, however, present a second possible strategy in that one can divide a long run into a series of overlapping segments. The total amount of time the sample is exposed to radiation in a long run is determined by the number of frequencies, integration time, and number of averages. Complex mixtures require large numbers of data points in order to recover the correct answer. As such, a total of 39 frequencies ranging from 0.5 to 274.5 MHz (allowing measurement of both long and short lifetimes) was chosen for this study. Five averages were collected at each frequency. Two integration times were chosen for the long run. A longer integration time of 30 s exposed the sample to 58.50 min of light and was used in dye mixture validation studies in order to increase the photobleaching. Dividing the integration time in half reduced exposure to 29.25 min and was used in lifetime measurements of the pyrene-SRFAR system in order to minimize the photobleaching. In order to reduce the total amount of time samples are exposed to radiation, the long run was divided into four different overlapping segments. The integration times were adjusted so that no point was exposed to more than 10 min of radiation (Table 1). A fresh solution was used in the measurement of each segment, and the data from four segments were recombined onto a single frequency-domain data set for analysis. The reduction of errors associated with photobleaching justifies the larger amount of sample required. This work presents the realization of this approach (1) in terms of a proof of concept on a model system, and (2) in a real world application.

Proof of concept on a model system

The model system A simple two component model system consisting of Fl and RhB was used to develop and evaluate the segmental approach to frequency-domain fluorescence lifetime measurements. The Fl and RhB dyes were chosen because they fluoresce in the same solvent system, can be excited at the same wavelength, photobleach differently, and have different lifetimes. Figure 1 clearly shows different behavior for these two dyes in terms of their susceptibility to photobleaching. Figure 1a also shows that both Fl and RhB were slightly dimmer (92.34 and 94.68% of their individual intensities, respectively) in the mixture compared to individual components—an effect attributable to the dynamic collision between these dyes [See Supplementary information (SI), Fig. 1S]. Figure 1b illustrates the progression of photobleaching for Fl and RhB within the mixture over a 30 min time span (see discussion below) and clearly shows that the intensity of Fl in the dye mixture decreased by approximately 55% after exposure to radiation, while the intensity of RhB shows minimal to no loss.

The results in Fig. 1 demonstrate that a Fl and RhB mixture is a multi-component system with a relatively large

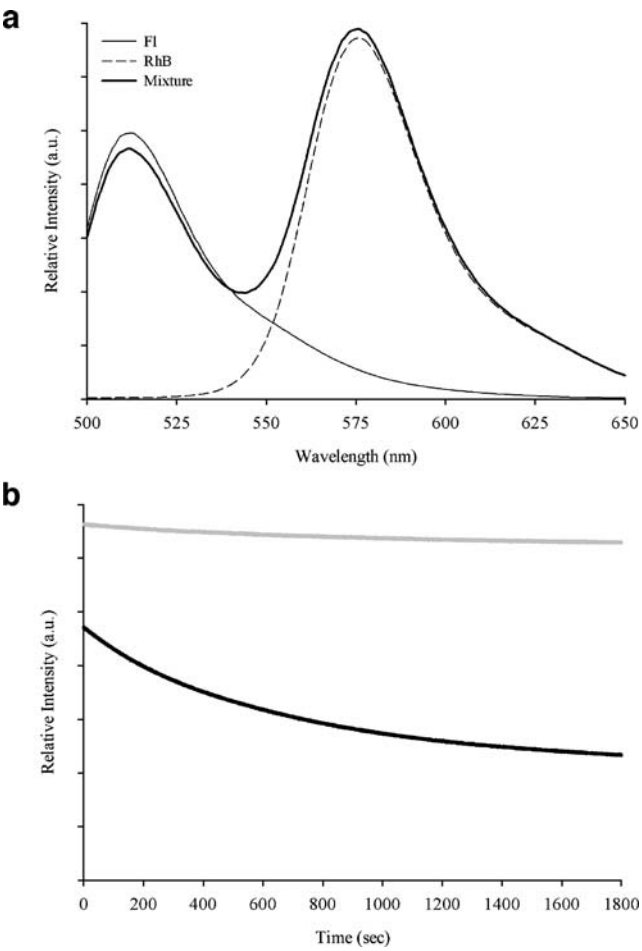

Fig. 1 **a** Fluorescence emission spectra of Fl (0.02 μM), RhB (1 μM), and mixture in 0.1 M NaOH excited at 490 nm and **b** time-based fluorescence steady-state experiments of the dye mixture excited at 490 nm and monitored at 512 nm (black solid line) and 576 nm (gray solid line) of Fl and RhB emission wavelengths, respectively

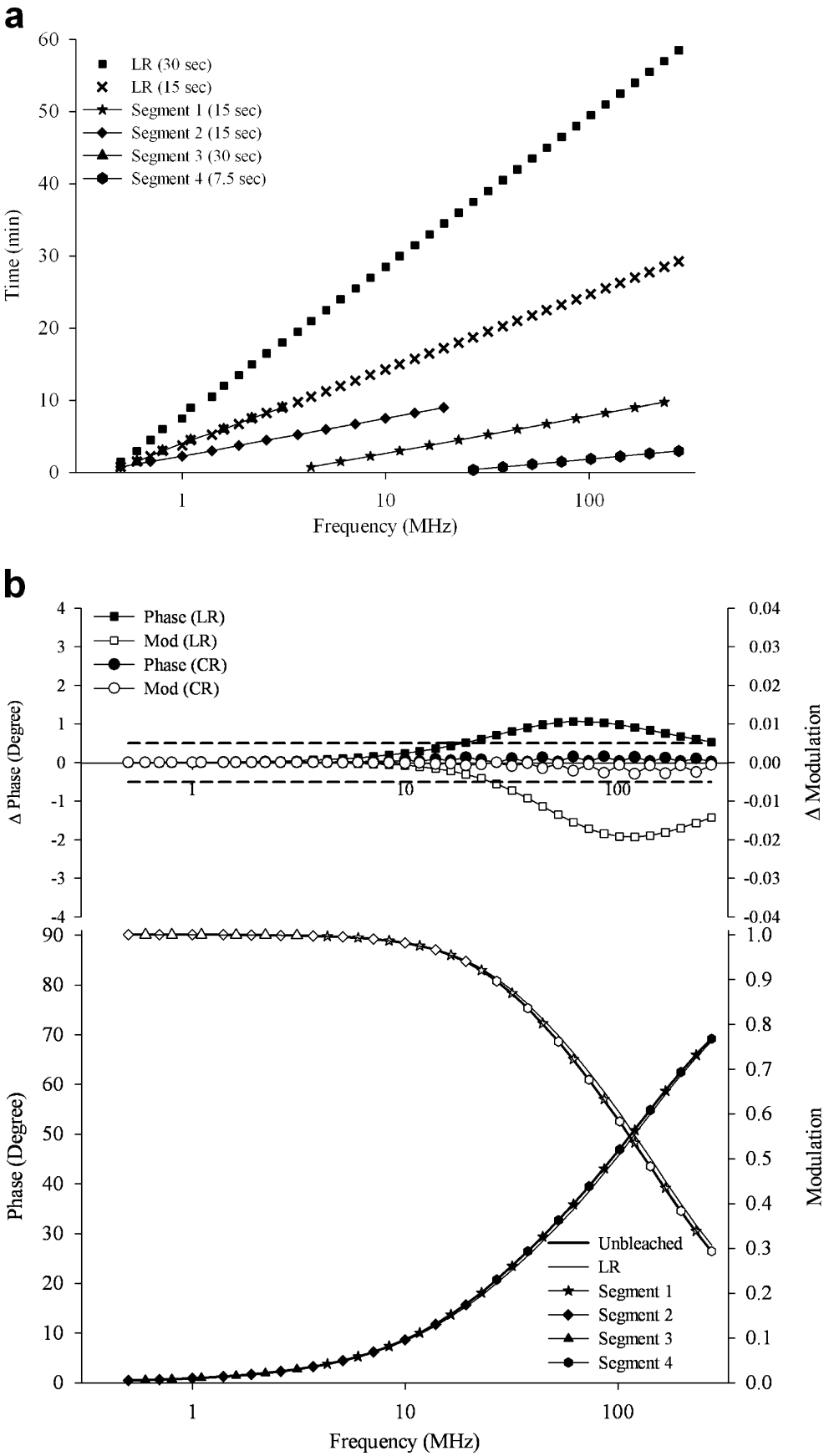

Fig. 2 **a** Exposure time as a function of frequency for the LR and four CR segments. **b** Simulated frequency-domain LR and CR data for Fl (τ=4.07 ns, $\alpha_{initial}$=0.420) and RhB (τ=1.30 ns, $\alpha_{initial}$=0.580) mixture. A 20% Fl photobleaching was assumed in the time the LR was exposed to radiation. Solid symbols in **b** represent phase. Open symbols in **b** represent modulation. Dashed lines in the residual plot represent the 0.5° and 0.005 modulation error values used in the NLLS analyses

amount of bleaching for one component and allows one to study the effect of photobleaching on lifetime measurements and the effectiveness of frequency segmentation and recombination. Figure 2a graphically represents the exposure of a sample to radiation as a function of integration time during the acquisition of data for a single long run (LR) or frequency segmentation and recombination, combined run (CR). From this figure it can be seen that frequency segmentation reduces the sample's exposure to radiation, while at the same time sampling the same frequency-domain. It should be noted, however, that modulation of the excitation light reduces the intensity of radiation that reaches the sample as compared to a steady-state measurement. Therefore, the mixture is exposed to less radiation in a frequency-domain lifetime measurement than in a steady-state measurement of equal time. The dye mixture used in the LR lifetime measurement is exposed to radiation for nearly twice as long as the mixture used in the steady-state experiment. Accordingly, values of 20 and 50% fluorescence intensity decrease were chosen for the simulations.

Simulations Figure 2b shows a simulated frequency-domain data set (phase and modulation as a function of frequency) for the LR dye mixture, assuming that Fl was photobleached by 20%. Real and imaginary portions of the signal were calculated using Eqs. 3 and 4, respectively. Fl and RhB lifetimes used in the simulation were those measured for the individual components, at 4.07 and 1.30 ns, respectively (Table 2). The initial fractional intensity of Fl was taken to be 0.420 based on the fractional intensity of Fl calculated from the steady-state emission spectrum of the mixture (Fig. 1a). An assumption was made that the intensity of the bleached component would decrease linearly with exposure time. The initial fractional intensity of Fl at 0.5 MHz (time=0 min) was 0.420 and decreased to 0.367 at 275.4 MHz (time=58.50 min). Therefore, a different set of fractional intensity values was used in Eqs. 3 and 4 for each modulation frequency. The outputs of Eqs. 3 and 4 were used in Eqs. 1 and 2 to calculate phase and modulation as a function of frequency. The individual segments of the CR were also simulated as above, with the fractional intensity contributions used in Eqs. 3 and 4, taking into account the reduced exposure to light (<10 min).

The results for these simulations are plotted in Fig. 2b along with their residuals (difference between unbleached and simulated data). It is clear from Fig. 2b that the simulated LR and unbleached run deviate from each other, especially at the higher modulation frequencies where the sample has been exposed to the greatest amount of light. A comparison of the CR with LR and unbleached run shows that errors resulting from photobleaching in the CR are much smaller than those for the LR. In fact, the errors caused by photobleaching in the CR are less than 0.5° and 0.005 modulation (the values used in our NLLS lifetime

Table 2 Recovered fluorescence lifetimes and fractional contributions obtained from NLLS analyses of the individual Fl and RhB components and their mixture

Model	Floating no.	Set	α_1	τ_1 (ns)	α_2	τ_2 (ns)	χ^2
D (V)	1	Fl (LR)	1.000	4.07	–	–	1.68
D (V)	1	RhB (LR)	1.000	1.30	–	–	2.29
D (V)	1	Mixture (LR)	1.000	1.89	–	–	32.81
		Mixture (CR)	1.000	1.99	–	–	23.40
DD (VVFV)	3	LR1	0.405	3.79	0.595	1.19	1.07
		CR1	0.413	3.69	0.587	1.29	0.93
DD (FVFV)	2	LR2	**0.420**	3.71	**0.580**	1.17	1.05
		CR2	**0.420**	3.65	**0.580**	1.29	0.92
DD (VFFF)	1	LR3	0.343	**4.07**	0.657	**1.30**	1.48
		CR3	0.377	**4.07**	0.623	**1.30**	1.34
DD (VFFF)	1	LR4	0.393	**3.76**	0.607	**1.23**	1.25
		CR4	0.430	**3.76**	0.570	**1.23**	1.34
DD (FFFF)	0	LR5	**0.420**	**4.07**	**0.580**	**1.30**	9.51
		CR5	**0.420**	**4.07**	**0.580**	**1.30**	3.81
DD (FFFF)	0	LR6	**0.420**	**3.76**	**0.580**	**1.23**	2.19
		CR6	**0.420**	**3.76**	**0.580**	**1.23**	1.45
DD (FFFF)	0	LR7	**0.413**	**3.69**	**0.587**	**1.29**	4.01
		CR7	**0.413**	**3.69**	**0.587**	**1.29**	0.89
DD (VFFF)	1	LR8	0.374	**3.69**	0.626	**1.29**	2.33
		CR8	0.413	**3.69**	0.587	**1.29**	0.90
DD (FVFV)	2	LR9	**0.413**	3.75	**0.587**	1.18	1.04
		CR9	**0.413**	3.69	**0.587**	1.29	0.92

Bolded black parameters are fixed values.

analyses for consistency and ease of day-to-day data interpretation). These results strongly suggest that, in practice, the frequency segmentation and recombination method will reduce errors associated with changing fractional intensity contributions within the multi-component system.

Measurements and NLLS analyses Simulations were compared to experimental LR and CR data in order to examine the effect of photobleaching. In addition to the 20% Fl photobleaching described above, 50% Fl, 20% RhB, and 50% RhB photobleaching were simulated for comparison. These simulations are shown together with experimental LR and CR data in Fig. 3. The experimental LR data's deviation from simulated unbleached data is indicative of the Fl component being photobleached, in agreement with the steady-state data. In contrast, CR experimental data matched more closely the simulated unbleached run, indicating that the frequency segmentation and recombination method reduces the effect of photobleaching.

The NLLS analyses of experimental data further support the above findings, as illustrated by the data presented in Table 2 for Fl (LR) and RhB (LR) as well as LR and CR data for their mixture. It is clear that a single-exponential decay model (D) does not fit experimental data for either the LR or CR of the mixture, as structured residuals and unreasonable χ^2 values were obtained. A double-exponential decay model (DD) was found to provide acceptable fits of the mixture for both LR and CR data. NLLS fitting using the DD model was examined by allowing some or all lifetimes and fractional contributions to vary (V) or by keeping these parameters fixed (F). Excellent fits and χ^2 values were obtained for both LR and CR data when all

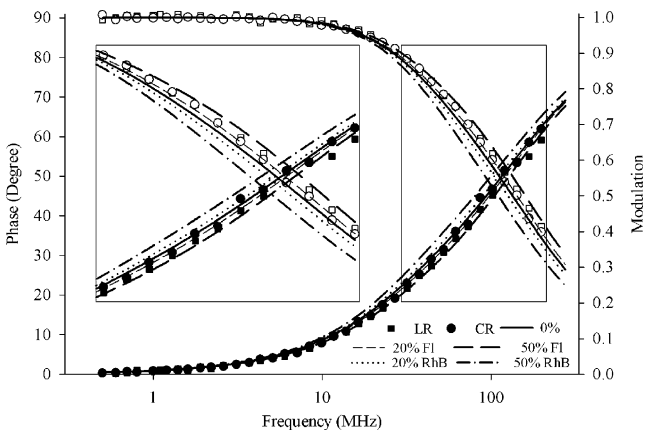

Fig. 3 Experimental and simulated frequency-domain LR and CR data for Fl (0.02 μM) and RhB (1 μM) mixture. Solid symbols represent phase. Open symbols represent modulation. Simulated frequency-domain LR data of the Fl (τ=4.07 ns, $\alpha_{initial}$=0.420) and RhB (τ=1.30 ns, $\alpha_{initial}$=0.580) mixture were simulated assuming (0%, 0%), (20%, 0%), (50%, 0%), (0%, 20%), (0%, 50%) photobleaching for Fl and RhB, respectively

parameters were allowed to vary (LR1 and CR1). However, recovered lifetimes and fractional contributions did not match. The Fl fraction for LR1 was slightly lower than that of CR1, possibly indicating the effect of photobleaching on the LR. In addition, the recovered RhB lifetime is shorter in LR1 than CR1 indicating that NLLS analysis may compensate for bleaching of one component by changing the recovered lifetime of the other.

In order to investigate the above effect, the data were analyzed with the lifetimes fixed at the measured lifetimes of individual components (LR3 and CR3). Reasonable χ^2 values were obtained for both. However, the results show that the NLLS analysis compensated for Fl photobleaching by reducing the Fl fraction for the LR3 compared to CR3. This was observed with the first trial, but more pronounced with the lifetimes fixed.

In order to further investigate how NLLS analysis compensates for photobleaching in frequency-domain lifetime measurements, the analyses were performed by fixing all parameters (LR5 and CR5). The lifetimes remained fixed at measured values for the individual components while the fraction of Fl was fixed at 0.420 based on the emission spectrum of the dye mixture (Fig. 1). An unacceptable χ^2 value of 9.51 was obtained for the LR, while a better but still high χ^2 value of 3.81 was obtained for the CR. Figure 4a and b show the fits and residuals for the LR and CR data, respectively. The residuals for both data fits show structure. This is likely caused by a mismatch between the lifetime values fixed in the analyses and the true lifetime values for the system. Recall that Fl and RhB were dimmer in their mixture than their individual components (Fig. 1), indicating that Fl and RhB lifetimes may have been affected by collisional quenching in the dye mixture.

Derivation of the Stern–Volmer equation reveals that the ratio of fluorescence lifetimes is equal to the ratio of fluorescence intensities in the absence and presence of the quencher, which can be expressed as follows [1]:

$$\frac{F_o}{F} = \frac{\tau_o}{\tau} \tag{8}$$

where F_o and F are fluorescence intensities and τ_o and τ denote lifetimes of the fluorophore in the absence and presence of the quencher, respectively. Consequently, Fl and RhB measured lifetimes were corrected for dynamic collisions in the mixture using Eq. 8. These corrected lifetimes (Fl=3.76 ns, RhB=1.23 ns) are similar to lifetimes recovered from CR1 with all parameters floating, further confirming our assertion that more confidence should be placed in the CR analysis than the LR analysis above. The Fl fraction and corrected lifetimes were fixed in the analyses of both LR6 and CR6 sets. NLLS analyses with lifetimes fixed at values estimated considering the effect of dynamic quenching result in better χ^2 values and residual

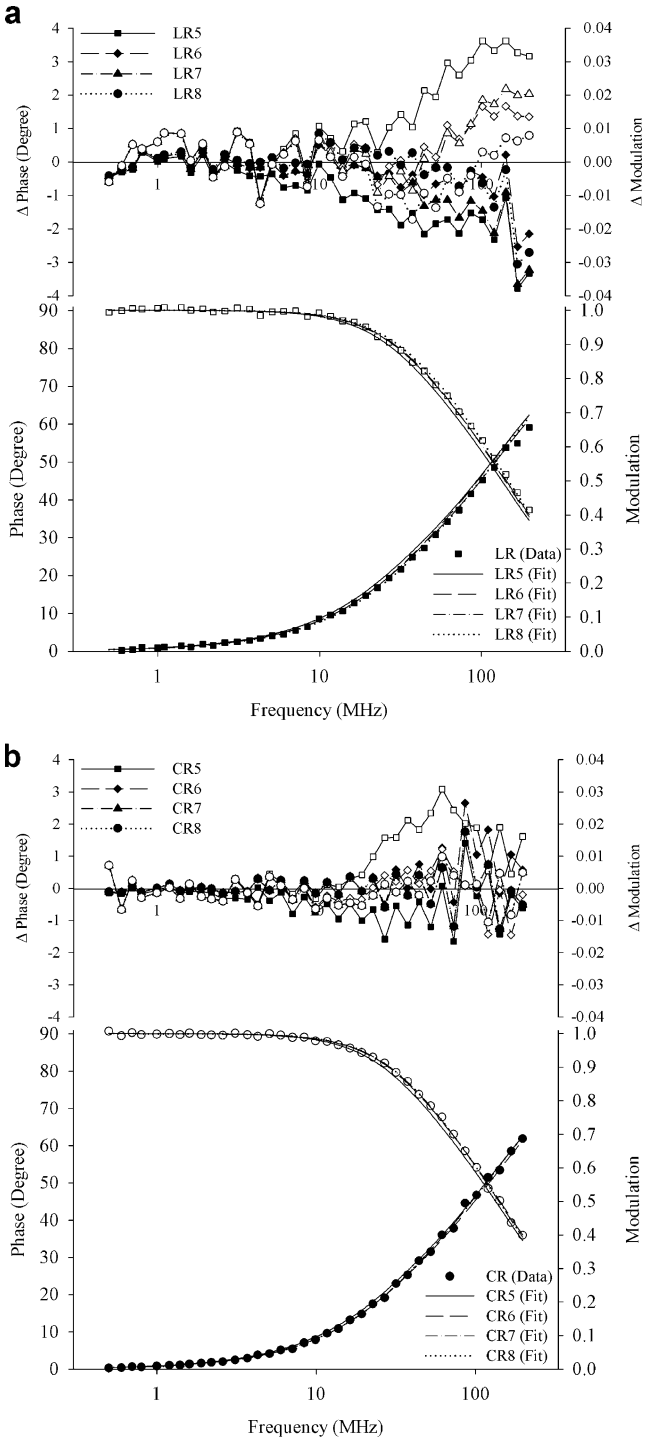

Fig. 4 **a** LR and **b** CR experimental frequency-domain data and NLLS fits for Fl (0.02 μM) and RhB (1 μM) mixture. Solid symbols represent phase. Open symbols represent modulation. Corresponding fitting parameters are tabulated in Table 2

plots, as illustrated in Table 2 and Fig. 4, particularly for analyses with the CR.

Proceeding with the assumption that the results from the CR analysis with all variables floating (CR1) most closely represent the true values, these values were fixed for comparison (LR7 and CR7). It is interesting to note that the LR7 fit worsened as compared to LR6 described above, as evidenced by an increase in the χ^2 value (Table 2) as well as the order within the residuals (Fig. 4a). The RhB lifetime for LR7 was longer than that used in LR6, providing more evidence that NLLS analysis compensates for Fl photobleaching by shortening the recovered RhB lifetime. In contrast, CR7 χ^2 improved compared to CR6. Most importantly, χ^2 for CR7 was much lower (0.89) compared to the LR7 (4.01), and the order within LR7 residuals in Fig. 4a was absent within CR7 residuals in Fig. 4b.

As a final test, Fl and RhB lifetimes were fixed at CR1 values, and the fractions were left to float (LR8 and CR8). NLLS analyses gave more reasonable χ^2 values with a lower Fl fraction for the LR compared to the set 6 results discussed above (Table 2 and Fig. 4). This LR8 fit, however, was worse than that of the LR1 where all parameters were allowed to float. These results indicate that LR data can be fit well with NLLS analysis when all parameters are left to float; however, recovered values may not represent the correct answer. When fixing the lifetimes (or fractions) at what were believed to be the correct values, the analysis adjusted the fractions (or lifetimes) to give the best fit possible. In both cases the resulting fits were worse than fits allowing all parameters to float. Problems associated with fitting LR data were eliminated as seen in the CR analyses presented in Table 2.

In general, residuals of the CR randomly oscillated around zero in both phase and modulation data, while those for the LR showed structure. The larger errors in residual plots of the CR observed at higher frequencies may be due to instrumental limitations. The largest standard deviations in the five averages collected at each frequency were observed at higher modulation frequencies for all LR and CR experiments. It should also be noted that segments 1 and 4 were mixed together to interrogate the high frequency region of the CR (Fig. 2a). Segment 4 has the shortest integration time and is expected to yield the largest amount of noise. It can also be seen in the simulated data (Fig. 2b) that despite segmentation and recombination having nearly eliminated the effect of photobleaching, the small remaining effect is the greatest at highest frequencies. In aggregate, these errors resulted in the largest residuals at highest frequencies in the CR. The fact that CR errors oscillate about zero indicates that no systematic errors were introduced.

"Real world" application: the association of pyrene with SRFAR

Experimental data Frequency-domain lifetime measurements via frequency segmentation and recombination were also applied to a more complex system consisting of a pyrene-SRFAR mixture. Individual component lifetimes

(pyrene and SRFAR) in argon degassed aqueous solutions were measured. The results are tabulated in Table 3 (See S1, Figs. 2S and 3S). The pyrene lifetime of 193.74 ns is in agreement with other reports of pyrene lifetime in an aqueous degassed solution [28]. The triple-exponential decay model (DDD) used to fit the data for the SRFAR solution is consistent with multi-exponential lifetimes reported for dissolved organic materials [29–31].

Table 3 summarizes a series of different discrete models used in NLLS analyses of experimental LR and CR data for the pyrene-SRFAR mixture. The most reasonable fits were obtained with models containing four lifetime components. It is reasonable to expect the mixture to display a minimum of four lifetimes consisting of the three SRFAR and one pyrene lifetime. A four-exponential decay model (DDDD) allowed a total of seven fitting parameters to float. A second simpler model ($D_fD_fD_fD$) kept SRFAR lifetimes fixed (f) reducing the number of variable parameters to 4. The final model, $(D+D+D)_FD$, held *both* the SRFAR fractions and lifetimes fixed (F) at measured values for SRFAR alone within the sum of three-exponential decays $(D+D+D)_F$ and allowed the pyrene fraction and lifetime to vary as a discrete (D) component model. This model reduced the total number of floating parameters to two. The $(D+D+D)_FD$ model was taken to be the most suitable model, assuming that SRFAR bulk fluorescence behavior is independent of pyrene's presence, and hence can be considered as a single component within a two component system.

As with the dye validation study, both LR and CR yielded different results. The validation study demonstrated that photobleaching of one component in a multi-component system gave misleading results for both lifetimes and fractions for analysis of the LR. The NLLS analyses of the pyrene-SRFAR mixture produced longer pyrene lifetimes for the LR compared to CR for all models evaluated (Table 3). Analyses using the DDDD model yielded nearly equal pyrene fractional contributions for both LR and CR. In addition, both SRFAR fractions and lifetimes of the CR were different from those obtained with the LR (See SI, Fig. 4Sa). Similar pyrene fractions were likely the result of the large number of floating parameters allowing SRFAR components to be adjusted to fit the LR data, as SRFAR lifetimes obtained from the CR were nearly the same as those for SRFAR individual component. The $D_fD_fD_fD$ model, where SRFAR lifetimes were fixed, recovered similar pyrene and SRFAR fractions for the LR and CR, but the floating SRFAR fractions again dominated the fit as indicated above (See SI, Fig. 4Sb). The $(D+D+D)_FD$ alleviated this problem by keeping all SRFAR parameters fixed. The experimental frequency-domain data for both LR and CR were fitted well with reasonable residual plots (Fig. 5a). The NLLS analyses of this model resulted in different lifetimes for both runs. The recovered pyrene lifetime (192.14 ns) with the LR was approximately 10 ns longer than that (181.89 ns) of the CR. The pyrene fraction was slightly lower for the LR compared to the CR indicating that pyrene photobleaching may be responsible for the different results. The difference in the measured pyrene lifetime between both runs can complicate the interpretation of the fluorescence quenching mechanism of pyrene in the presence of SRFAR.

Simulations Simulations were performed to confirm that a reduction in the pyrene intensity between the beginning and

Table 3 Recovered fluorescence lifetimes and fractional contributions obtained from NLLS analyses of pyrene, SRFAR, and their mixture

Model	Floating no.	Set	α_{SRFAR}	α_1	τ_1 (ns)	α_2	τ_2 (ns)	α_3	τ_3 (ns)	α_4	τ_4 (ns)	χ^2
D	1	Pyrene	–	1.000	193.74	–	–	–	–	–	–	0.72
D	1	SRFAR	–	1.000	3.07	–	–	–	–	–	–	466.59
DD	3	SRFAR	–	0.472	1.05	0.528	7.61	–	–	–	–	12.05
DDD	5	SRFAR	–	0.281	0.57	0.483	3.43	0.236	13.71	–	–	1.93
D	1	LR	–	1.000	6.66	–	–	–	–	–	–	1987.38
D	1	CR	–	1.000	6.74	–	–	–	–	–	–	1936.79
DD	3	LR	–	0.531	2.12	0.469	138.55	–	–	–	–	87.29
DD	3	CR	–	0.531	2.16	0.469	131.69	–	–	–	–	84.07
DDD	5	LR	–	0.266	0.90	0.335	6.38	0.399	178.93	–	–	3.78
DDD	5	CR	–	0.254	0.88	0.345	6.11	0.401	168.89	–	–	4.78
DDDD	7	LR	–	0.162	0.51	0.239	2.75	0.208	9.21	0.391	183.77	2.80
DDDD	7	CR	–	0.173	0.56	0.281	3.34	0.157	11.02	0.389	175.84	3.55
$D_fD_fD_fD$	4	LR	–	0.179	**0.57**	0.297	**3.43**	0.142	**13.71**	0.382	189.27	3.02
$D_fD_fD_fD$	4	CR	–	0.172	**0.57**	0.306	**3.43**	0.140	**13.71**	0.382	179.76	3.57
$(D+D+D)_FD$	2	LR	0.622	**0.281**	**0.57**	**0.483**	**3.43**	**0.236**	**13.71**	0.378	192.14	3.17
$(D+D+D)_FD$	2	CR	0.621	**0.281**	**0.57**	**0.483**	**3.43**	**0.236**	**13.71**	0.379	181.89	3.55

The f subscripts indicate the fits where SRFAR lifetimes were fixed during NLLS analyses. The F subscripts denote the fits where both SRFAR fractional intensity contributions and lifetimes were fixed during NLLS analyses. Bolded black parameters are fixed values.

end of the LR experiment resulted in differences between the LR and CR experimental data described above. Assuming the results from the $(D+D+D)_FD$ analysis of the CR experiment (Table 3) most closely represents the true values, these values were used to simulate this system in the same manner as previous simulations. The fluorescence intensity of pyrene was assumed to decrease linearly by 20%, while the fluorescence intensity of SRFAR remained constant. Simulated LR, CR, and unbleached run data are shown in Fig. 6a. A close examination reveals that there was a mismatch between the unbleached and LR simulated data. Once again, errors resulting from photobleaching in the LR are greatly reduced in the CR.

The NLLS analyses of simulated data files after addition of random noise (0.5° and 0.005) allowed the investigation of how pyrene photobleaching would affect the recovered parameters in a LR experiment. The simulation was performed ten times with different random noise of

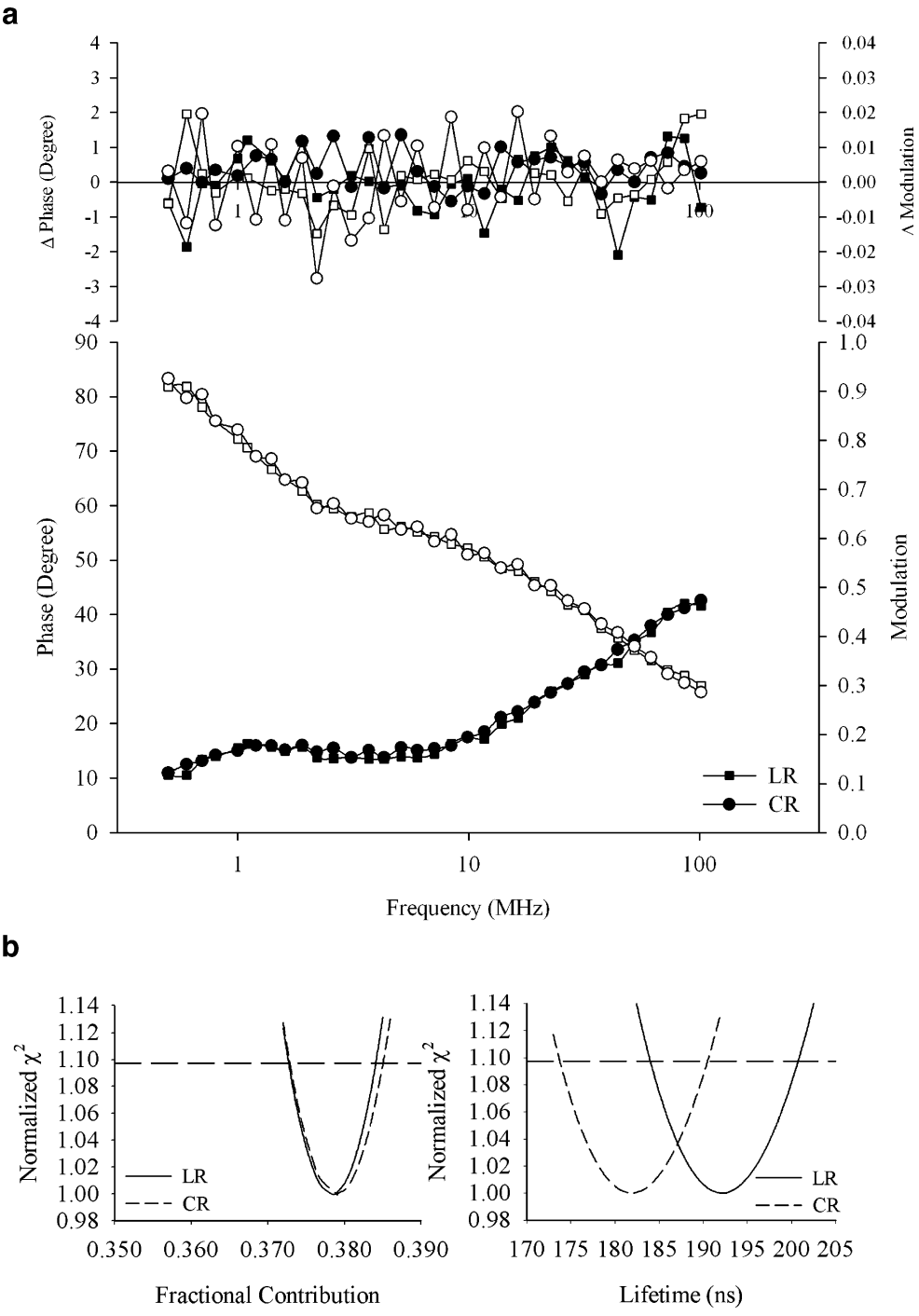

Fig. 5 **a** Experimental frequency-domain data and NLLS fits for pyrene (0.04 ppm) and SRFAR (12 ppm) mixture. Solid symbols represent phase. Open symbols represent modulation. **b** Normalized χ^2 surfaces for NLLS analyses of the experimental data. Horizontal dashed lines: one standard deviation from the minima of the χ^2 surface. Corresponding fitting parameters are tabulated in Table 3

equivalent magnitude added to each simulation (See SI for examples of simulated data with noise added). Recovered parameters for unbleached, LR, and CR simulations (ten simulated data files each) using the $(D+D+D)_FD$ model are tabulated in the SI (Table 1S). Results for global analyses of all files within each set are plotted as the χ^2 surfaces shown in Fig. 6b. Recovered parameters for the CR simulation matched more closely those of the unbleached simulated data than did those of the LR. For both experimental and simulated data, pyrene lifetimes recovered from the LR were approximately 10 ns longer than those recovered from the CR, while the pyrene fractions were lower. The agreement between the simulated and experimental data is shown by the similarity of Figs. 5b and 6b. Together, the

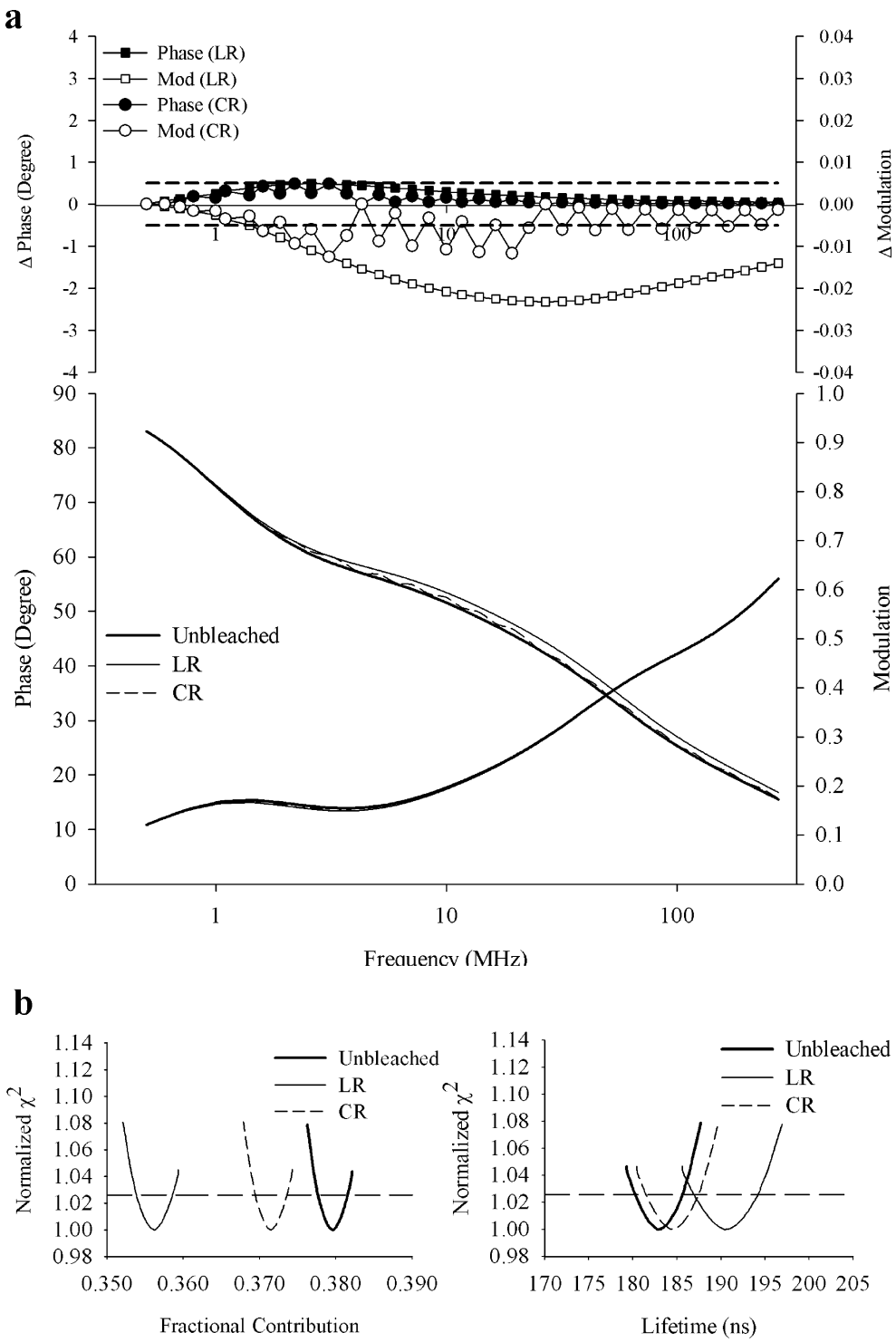

Fig. 6 **a** Simulated frequency-domain LR and CR data for pyrene (τ=181.89 ns, $\alpha_{initial}$= 0.379) and SRFAR ($\alpha_{initial}$= 0.621, τ_1=0.57 ns, α_1=0.281, τ_2=3.43 ns, α_2=0.483, τ_3= 13.71 ns, α_3=0.236) mixture. A 20% pyrene photobleaching was assumed in the time the LR was exposed to radiation. Solid symbols represent phase. Open symbols represent modulation. Dashed lines in the residual plot represent the 0.5° and 0.005 modulation error values used in the NLLS analyses. **b** Normalized χ^2 surfaces for NLLS analyses of the simulated data after 0.5° and 0.005 random noise was added. Horizontal dashed lines: one standard deviation from the minima of the χ^2 surface. Corresponding fitting parameters are tabulated in SI, Table 1S

experimental and simulated LR and CR data illustrate that a decrease in the pyrene intensity over the course of the LR measurement affect the recovered parameters.

Conclusions

The concept of frequency segmentation and recombination was demonstrated through both simulated and experimental data. The results from our experiments provide clear evidence that the frequency segmentation and recombination method reduced errors that result from a changing fractional contribution in a multi-component system. NLLS analyses of the dye mixture further confirmed these findings. Better fits, more reasonable χ^2 values, and more random residual plots were obtained from the CR compared to the LR.

In addition, this newly developed method was applied to a more complex system consisting of pyrene and SRFAR to improve recovered lifetimes and fractional contributions in a real-world multi-component system. Comparison of experimental data collected in traditional (LR) and segmented (CR) fashion with simulated results revealed that a mismatch between lifetimes recovered from LR and CR data was consistent with a decrease in pyrene intensity over the course of the experiment. This decrease is likely due to pyrene photobleaching, wall adsorption, or both, within the multi-component system. Frequency segmentation and recombination experiments appeared to minimize these potential factors and provide more reliable results. Finally, these results showed considerable promise for use of frequency-domain fluorescence lifetime measurements via frequency segmentation and recombination in a range of applications, including biological and environmental.

Acknowledgments Robert L. Cook acknowledges the Louisiana Education Quality Support Fund (LEQSF [2004-07]-RD-A-07). Isiah M. Warner acknowledges the National Science Foundation, the National Institutes of Health, and the Philip W. West Endowment for their support. Hadi M. Marwani expresses sincere gratitude to the King Abdulaziz University in Saudi Arabia for partial support during this study.

References

1. Lakowicz JR (1999) Principles of fluorescence spectroscopy, 2nd edn. Kluwer Academic/Plenum Press, New York
2. Ingle JD, Crouch SR (1988) Spectrochemical analysis, 1st edn. Prentice-Hall, Inc., Upper Saddle River
3. Sharma A., Schulman SG (1999) Introduction to fluorescence spectroscopy, 1st edn. John Wiley and Sons, Inc., New York
4. Van den Engh G, Farmer C (1992) Photo-bleaching and photon saturation in flow cytometry. Cytometry 13(7):669–677
5. Sandinson DR, Williams RM, Wells KS, Strickler J, Webb WW (1995) Quantitative fluorescence confocal laser scanning (CLSM). In: Pawley JB (ed) Handbook of biological confocal microscopy, 1st edn. Plenum Press, New York, pp 39–53
6. Nakamura K, Kowaki T, Scully AD, Hirayama S (1997) Quenching of chlorophyll a fluorescence by oxygen in highly concentrated solutions and microdroplets. J Photochem Photobiol A Chem 104(1–3):141–149
7. Druzhinin SI, Galievsky VA, Zachariasse KA (2005) Photoproduct formation with 4-aminobenzonitriles in acetonitrile and its effect on photophysical measurements. J Phys Chem A 109(49):11213–11223
8. Bopp MA, Jia Y, Li L, Cogdell RJ, Hochstrasser RM (1997) Fluorescence and photobleaching dynamics of single light-harvesting complexes. Proc Natl Acad Sci USA 94(20):10630–10635
9. Marcu L, Grundfest WS, Maarek J-MI (1999) Photobleaching of arterial fluorescent compounds: characterization of elastin, collagen and cholesterol time-resolved spectra during prolonged ultraviolet irradiation. Photochem Photobiol 69(6):713–721
10. Chen Y, Periasamy A (2004) Two-photon FLIM-FRET microscopy for protein localization. In: Periasamy Ammasi, So PTC (eds) Multiphoton microscopy in the biomedical sciences IV. Proc SPIE Int Soc Opt Eng 5323:431–439
11. Rueck A, Dolp F, Huelshoff C, Hauser C, Scalfi-Happ C (2005) FLIM and SLIM for molecular imaging in PDT. In: Periasamy A, So PT (eds) Multiphoton microscopy in the biomedical sciences V. Proc SPIE Int Soc Opt Eng 5700:182–187
12. Connelly JP, Botchway SW, Kunz L, Pattison D, Parker AW, MacRobert AJ (2001) Time-resolved fluorescence imaging of photosensitiser distributions in mammalian cells using a picosecond laser line-scanning microscope. J Photochem Photobiol A Chem 142(2–3):169–175
13. Fujimoto D, Akiba K, Nakamura N (1977) Isolation and characterization of a fluorescent material in bovine Achilles tendon collagen. Biochem Biophys Res Commun 76(4):1124–1129
14. Deyl Z, Macek K, Adam M, Vancikova (1980) Studies on the chemical nature of elastin fluorescence. Biochim Biophys Acta 625(2):248–254
15. Brustlein S, Devaux F, Wacogne B, Lantz E (2004) Fluorescence lifetime imaging on the picosecond timescale. Laser Phys 14(2):238–242
16. Lakowicz JR, Szmacinski H, Nowaczyk K, Berndt KW, Johnson M (1992) Fluorescence lifetime imaging. Anal Biochem 202(2): 316–330
17. Lakowicz JR, Szmacinski H, Nowaczyk K, Lederer WJ, Kirby MS, Johnson ML (1994) Fluorescence lifetime imaging of intracellular calcium in COS cells using Quin-2. Cell Calcium 15(1):7–27
18. Murata S-I, Herman P, Lin H-J, Lakowicz JR (2000) Fluorescence lifetime imaging of nuclear DNA: effect of fluorescence resonance energy transfer. Cytometry 41(3):178–185
19. Laor Y, Rebhun M (2002) Evidence for nonlinear binding of PAHs [Polycyclic Aromatic Hydrocarbons] to dissolved humic acids. Environ Sci Technol 36(5):955–961
20. Tiller CL, Jones KD (1997) Effects of dissolved oxygen and light exposure on determination of KOC values for PAHs using fluorescence quenching. Environ Sci Technol 31(2):424–429
21. Backhus DA, Golini C, Castellanos E (2003) Evaluation of fluorescence quenching for assessing the importance of interactions between nonpolar organic pollutants and dissolved organic matter. Environ Sci Technol 37(20):4717–4723
22. Chen S, Inskeep WP, Williams SA, Callis PR (1994) Fluorescence lifetime measurements of fluoranthene, 1-naphthol, and napropamide in the presence of dissolved humic acid. Environ Sci Technol 28(9):1582–1588
23. Holbrook RD, Love NG, Novak JT (2004) Investigation of sorption behavior between pyrene and colloidal organic carbon from activated sludge processes. Environ Sci Technol 38(19):4987–4994
24. Valeur B (2001) Molecular fluorescence: principles and applications, 1st edn. Wiley-VCH, Weinheirn
25. He Y, Geng L (2001) Analysis of heterogeneous fluorescence decays. Distribution of pyrene derivatives in an octadecylsilane layer in capillary electrochromatography. Anal Chem 73(22):5564–5575

26. Beechem JM, Gratton E (1988) Fluorescence spectroscopy data analysis environment: a second generation global analysis program. SPIE Proc Time-Resolved Laser Spectrosc Biochem 909:70–81
27. Beechem JM (1989) A second generation global analysis program for the recovery of complex inhomogeneous fluorescence decay kinetics. Chem Phys Lipids 50(3–4):237–251
28. Nelson G, Patonay G, Warner IM (1988) Effects of selected alcohols on cyclodextrin inclusion complexes of pyrene using fluorescence lifetime measurements. Anal Chem 60(3):274–279
29. Cook RL, Langford CH (1995) Metal ion quenching of fulvic acid fluorescence intensities and lifetimes: nonlinearities and a possible three-component model. Anal Chem 67(1):174–180
30. Hemmingsen SL, McGown LB (1997) Phase-resolved fluorescence spectral and lifetime characterization of commercial humic substances. Appl Spectrosc 51(7):921–929
31. Hewitt JD, McGown LB (2003) On-the-fly fluorescence lifetime detection of humic substances in capillary electrophoresis. Appl Spectrosc 57(3):256–265